# Satellites are closer than you think: A near field MIMO approach for Ground stations

Rohith Reddy Vennam[†], Luke Wilson[†], Ish Kumar Jain[§], Dinesh Bharadia[†]
[†]University of California San Diego, La Jolla, CA
[§]Rensselaer Polytechnic Institute, Troy, NY
Email: rvennam@ucsd.edu, l5wilson@ucsd.edu, jaini@rpi.edu, dineshb@ucsd.edu

***Abstract*—The rapid growth of low Earth orbit (LEO) satellite constellations has revolutionized broadband access, Earth observation, and direct-to-device connectivity. However, the expansion of ground station infrastructure has not kept pace, creating a critical bottleneck in satellite-to-ground backhaul capacity. Traditional parabolic dish antennas, though effective for geostationary (GEO) satellites, are ill-suited for dense, fast-moving LEO networks due to mechanical steering delays and their inability to track multiple satellites simultaneously. Phased array antennas offer electronically steerable beams and multi-satellite support. However, their integration into ground stations is limited by the high cost, hardware issues, and complexity of achieving sufficient antenna gain. We introduce *ArrayLink*, a distributed phased array architecture that coherently combines multiple small, commercially available panels to achieve high-gain beamforming and unlock line-of-sight MIMO spatial multiplexing with minimal additional capital expenditure. By spacing 16 32×32 panels across a kilometer-scale aperture, *ArrayLink* enters the radiative near-field, focusing energy in both angle and range while supporting up to four simultaneous spatial streams on a single feeder link. Through rigorous theoretical analysis, detailed 2D beam pattern simulations and real-world hardware experiments, we show that *ArrayLink* (i) achieves dish-class gain exceeding that of a 1.47 m reflector, (ii) maintains four parallel streams at ranges of hundreds of kilometers (falling to two beyond 2000 km), and (iii) exhibits tight agreement across theory, simulation, and experiment with minimal variance. These findings pave the way for a practical and scalable approach to boosting satellite backhaul capacity.**

***Index Terms*—Near-field MIMO, Coherent beamforming, Satellite ground stations, LEO Satellites, Satellite backhaul;**

## I. Introduction

The rapid growth of low Earth orbit (LEO) satellite constellations has fundamentally transformed broadband connectivity, Earth observation, and direct-to-device connectivity. Major players like SpaceX's Starlink, Planet Labs, Amazon Kuiper, and OneWeb [1]–[4] are deploying massive networks that underpin critical applications, from internet services to solar weather monitoring. However, the ground segment infrastructure has not scaled proportionally, creating a significant bottleneck in satellite-to-ground backhaul capacity. Overcoming this issue requires ground station architectures capable of delivering (1) *high throughput* to handle increasing data rates, (2) *resource efficiency* to quickly track and seamlessly transfer data between fast moving satellites, and (3) *scalability* to economically deploy numerous ground stations in response to expanding satellite constellations.

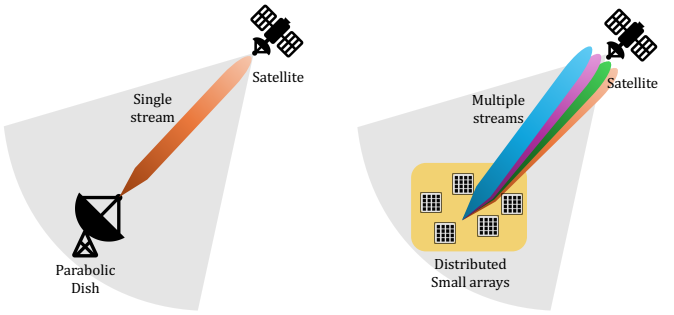


(a) Current satellite ground stations built using Parabolic Dishes.

(b) Proposed satellite ground stations with distributed phased arrays.

Fig. 1: An illustration of satellite to earth ground station links: (a) current approach (b) proposed approach

**Parabolic dish antennas** remain the backbone of satellite ground stations for high-gain feeder links, providing reliable, focused beams. For example, SpaceX employs 1.47 m and 1.85 m dishes, achieving gains of 49.5 and 52.6 dBi, respectively [5], [6]. However, these dishes are inherently inflexible, as each can only track one satellite at a time. Mechanical steering is required to maintain alignment with rapidly moving LEO satellites, resulting in significant downtime during satellite handoffs. For instance, Intelsat dishes rotate at speeds of only $2-5^\circ$ per second, causing transitions from $-60^\circ$ to elevation $+60^\circ$ to take nearly a minute, during which the station is temporarily unavailable. These constraints lead to inefficient resource utilization. Furthermore, deploying additional parabolic dishes to scale capacity significantly increases land, power, and backhaul costs, making traditional dish architectures unsuitable for meeting the flexibility and scalability demands of modern LEO constellations.

**Large phased arrays** offer a promising alternative, enabling beam hopping in microseconds and supporting multiple links simultaneously without mechanical parts [7]. Despite these advantages, their integration into ground stations faces significant challenges. Achieving a high antenna gain comparable to a 1.85 m Starlink class dish (52.6 dBi [6]) would *require a large array with more than 50,000 elements*. Such massive monolithic arrays lead to prohibitive power consumption, complex thermal management, and high manufacturing costs, severely limiting their current field deployment. Consequently, neither traditional parabolic dishes nor large phased-array

architectures effectively meet the flexibility, scalability, and performance demands of next-generation LEO ground stations.

***ArrayLink*:** To overcome these limitations, we introduce *ArrayLink*, a novel distributed phased-array ground station that coherently links many small phased-array panels spread across a large area into a single high-performance system. By efficiently combining multiple affordable and commercially available arrays, *ArrayLink* delivers high beamforming gains and simultaneously unlocks multiple concurrent data streams, transforming satellite ground station connectivity. Specifically, *ArrayLink* addresses all three critical requirements: (1) achieves *high link throughput* by delivering high-gain links and allowing multiple streams (2) the inherent electronic beam-steering capability of phased arrays allows rapid satellite tracking and *efficient spectrum utilization*, eliminating downtime associated with mechanical steering; (3) leveraging mass-produced phased-array panels developed originally for user terminals and in-flight connectivity drastically reduces deployment costs and enables rapid scalability.

To achieve high-speed, scalable backhaul connectivity, *ArrayLink* addresses two fundamental challenges:

- **Achieving Cost-Effective High-Gain Links:** A key barrier for phased arrays in ground-station architectures is matching the high gain provided by large dishes; for instance, SpaceX's 1.85 m dishes achieve 52.6 dBi [6]. Achieving similar gain with phased arrays traditionally requires over 50,000 antenna elements, making monolithic arrays expensive and complex. Our key observation is that antenna gain increases logarithmically with the number of elements—rapidly rising initially but flattening with larger counts. Rather than building prohibitively large arrays, we combine a modest commercially available phased-array panels. For example, by coherently combining *16 off-the-shelf arrays* (each with about 36.1 dBi), *ArrayLink* achieves approximately 48.1 dBi. To bridge the remaining gap ( 4.5 dB) without inefficiently adding more elements, we leverage digital multiple-input multiple-output (MIMO) techniques to enable multiple simultaneous data streams, maximizing throughput while controlling costs and making phased array systems feasible.
- **Enabling Multi-Stream MIMO in LoS Channels:** Conventional satellite links operate primarily in a Line-of-Sight (LoS) environment, leading to highly correlated MIMO channels that are unsuitable for spatial multiplexing. However, in near-field conditions, each antenna experiences distinct phase variations, transforming the channel into a suitable one for MIMO. However, the key challenge here is *"how to enable these near-field conditions at practical satellite distances"*. To address this, we developed a novel mathematical model that precisely characterizes near-field MIMO feasibility, showing explicitly how adjusting transmit and receive aperture sizes can control the near-field region. Leveraging this model, we distribute phased-array panels across a kilometer-scale aperture, enabling robust near-field LoS MIMO and supporting multiple concurrent streams to satellites at distances up to 2,000 km, all while maintaining high individual link gains (48.1 dBi).

Further, we discuss how to reduce grating lobes and achieve coherent combining in our design section. We validate the effectiveness of *ArrayLink* through a rigorous evaluation, combining theoretical insights, high-fidelity simulations, and real-world hardware experiments. First, we derive analytical models that precisely characterize singular values, degrees of freedom, and define clear boundaries for near-field MIMO feasibility based on transmit and receive aperture sizes. Next, we perform outdoor hardware experiments with a 2×2 MIMO setup at 27 GHz, testing various aperture sizes and ranges from 2.5 m to 100 m. Remarkably, our hardware measurements closely align with both theoretical predictions and simulation results, demonstrating the accuracy and robustness of our simulator and mathematical models. Finally, extensive satellite-to-ground station link simulations confirm that *ArrayLink* coherently focuses beams in both angle and distance, achieving individual link gains of approximately 48.14 dBi. Notably, our results show the ability to sustain up to four simultaneous data streams at hundreds of kilometers and at least two streams at ranges beyond 2,000 km, highlighting *ArrayLink*'s powerful capability to transform satellite ground-station connectivity.

**Contributions.** We summarize our contributions as follows:

1) ***ArrayLink* architecture:** A novel and scalable ground station design that coherently combines multiple small phased array panels to enable high-gain, multi-stream feeder links.
2) **Near-field MIMO modeling:** An analytical framework that characterizes the feasibility of spatial multiplexing in LoS channels and demonstrates how aperture dimensions can be tuned to achieve near-field MIMO at satellite-scale distances.
3) **Coherent beamforming:** A practical delay-compensation technique that enables phase-coherent combining across distributed panels while mitigating grating lobes through aperiodic panel placement.
4) **Open-source tools and datasets:** A publicly released python-based simulator for near-field MIMO along with a real-world hardware dataset (captured at 27 GHz over 2.5–100 m), supporting reproducibility and future research in LoS MIMO. Our implementation and channel datasets are available at link (github.com/ucsdwcsng/ArrayLink.git).

## II. Background and Related Work

### A. Background on Satellite ground station geometry

***Parabolic Dish Ground Stations:*** Parabolic dish antennas have long served as the standard architecture for satellite ground stations due to their high directivity and aperture efficiency. The antenna gain $G$ is given by [8]

$$G = \frac{4\pi A}{\lambda^2} e_A = \left(\frac{\pi D}{\lambda}\right)^2 e_A,$$

where $D$ is the dish diameter, $\lambda$ the wavelength, and $e_A$ the aperture efficiency (typically 0.5–0.7). For example, a 1.47 m

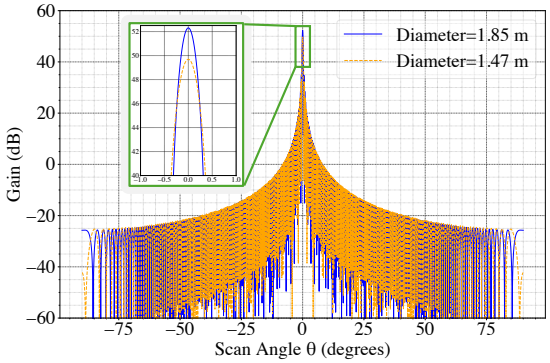


Fig. 2: Gain pattern of a 1.85m (max 52.6 dBi) and 1.47m (max 49.5 dBi) parabolic dish antenna operating at 28 GHz.

parabolic dish operating in the Ka band (28 GHz) achieves approximately 49.5 dBi gain, sufficient to support Starlink LEO constellations [5]. As illustrated in Fig. 2, the measured gain pattern closely approaches 48.1 dBi for a 1.47 m dish and 52.6 dBi for a 1.85 m dish at 28 GHz.

Despite their high gain, parabolic dishes rely on mechanical steering to track LEO satellites moving at approximately 7.6 km/s. Continuous reorientation introduces latency, handover interruptions, and operational complexity. Satellite transitions can require angular movements exceeding 120°, which may take several seconds to a minute depending on dish size [9]. At millimeter-wave frequencies, precise pointing is critical; even small angular errors can cause significant signal degradation and increased interference [10], [11]. These constraints lead to periods of link unavailability and underutilized ground-station resources.

***Phased Array Antennas:*** Phased array antennas provide electronically steerable beams without mechanical motion by adjusting the relative phases of $N$ radiating elements. The resulting directional gain depends on both the element radiation pattern and the array factor [12]. For a rectangular $M \times N$ array with element spacings $d_x$ and $d_y$, the array factor is

$$AF(\theta,\phi) = \sum_{m=0}^{M-1}\sum_{n=0}^{N-1} w_{mn} e^{jk[md_x \sin(\theta)\cos(\phi)+nd_y \sin(\theta)\sin(\phi)]}, \quad (1)$$

where $w_{mn}$ are the beamforming weights and $k = 2\pi/\lambda$ is the wavenumber. Phased arrays enable rapid beam steering (< milliseconds) and can form multiple independent beams to simultaneously track several satellites [12]. However, scaling phased arrays to ground-station-class gains remains challenging. Achieving gains above 52.6 dBi at 28 GHz requires tens of thousands of antenna elements (e.g., 50,000+ elements at ~ 6 dBi per element), leading to high power consumption, thermal management challenges, mutual coupling effects, and substantial manufacturing cost.

In summary, parabolic dishes provide high gain but limited agility, while phased arrays offer agility at the expense of increased complexity and cost. Neither approach alone satisfies the scalability and performance demands of next-generation LEO ground stations.

### B. Related work

**Line-of-Sight MIMO:** Recent work on near-field wireless systems investigates beam focusing and channel estimation for extremely large aperture arrays, exploiting spherical wavefront propagation under a variety of analog and hybrid beamforming architectures [13]–[19]. Other studies extend near-field models to reconfigurable intelligent surfaces (RIS) [20] and integrated sensing-and-communication (ISAC) systems [21]. Several surveys formalize Rayleigh and Fresnel distance definitions and introduce Fresnel-zone beam focusing [22], [23]. While these works establish the theoretical foundations of near-field propagation, they do not examine how antenna placement under hardware constraints impacts channel rank, capacity, or grating lobes behavior.

Classical LoS MIMO studies instead improve channel rank through geometry. Prior work shows that carefully spaced uniform planar arrays can achieve full multiplexing gain in far-field LoS channels [24], [25]. However, scaling these designs to satellite ground stations requires thousands of antennas, leading to prohibitively high costs, excessive power consumption, and severe grating-lobe challenges. At the network level, distributing satellites across orbital planes can increase channel rank [26], but the complexity of ground stations remains unchanged. To the best of our knowledge, no prior work applies near-field LoS MIMO principles to support multiple streams to a single satellite feeder link.

**Phased-array ground stations.** Several recent efforts explore replacing parabolic dishes with electronically steerable phased arrays. [27] combines a small phased array with a passive metasurface to improve link budget, while [28] employs compact uniform arrays with Rotman lenses for indoor satellite reception. Large planar phased arrays for Starlink-class gateways are evaluated in [29] through electromagnetic simulations, and [30] surveys AI-assisted beam tracking for LEO terminals. These designs focus primarily on far-field beam steering, gain enhancement, or tracking accuracy, and rely on dense, uniformly spaced arrays. In contrast, *ArrayLink* applies near-field LoS MIMO principles to satellite ground stations using a sparse, distributed phased-array architecture. By randomizing panel placement and jointly optimizing per-panel phase control, *ArrayLink* simultaneously preserves near-field spatial multiplexing gains and suppresses grating lobes, achieving high capacity with an order of magnitude fewer antennas than uniform designs.

Prior work demonstrates that distributed antennas can be synchronized with a timing accuracy of 2.36 – 20.0 picoseconds [31], [32] and accurate phase sync. As synchronization is no longer the primary bottleneck, this work focuses on how array geometry and antenna placement enable near-field LoS MIMO gains under practical hardware constraints.

## III. Design

To address the limitations of both parabolic dishes [5], [6] and monolithic large phased arrays [7] as ground stations, we design *ArrayLink*, a *distributed phased-array architecture*. As shown in Fig. 3, *ArrayLink* aggregates multiple smaller

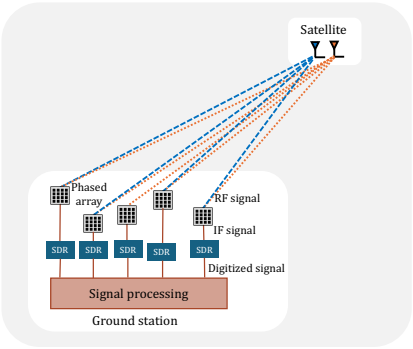


Fig. 3: ***ArrayLink* architecture:** Distributed phased arrays downconvert the RF signal to IF, which is then digitized by SDRs. The digitized streams from multiple arrays are jointly processed to enable MIMO and coherent combining.

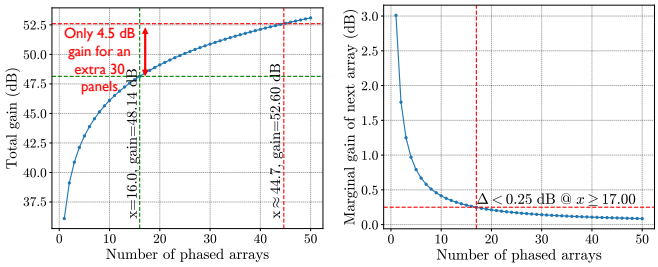


(a) Total gain as a function of the number of phased arrays.

(b) Marginal gain contributed by each additional array.

Fig. 4: Tradeoff in array aggregation: while more arrays increase total gain, marginal improvements diminish sharply beyond 16 panels.

phased-array panels into a coordinated network. To achieve our goal of enabling high-throughput backhaul links while ensuring practical feasibility and cost-effectiveness, the design of *ArrayLink* focuses on four key aspects: (i) combining smaller arrays to achieve high gain, (ii) leveraging distributed coordination to enable near-field MIMO, (iii) characterizing the boundaries of the feasible MIMO region, and (iv) determining array placements that mitigate grating lobes.

### *A. Aggregating Smaller Phased Arrays for High-Gain Links*

To enable high-gain satellite links, ground stations have traditionally relied on parabolic dishes, whose large physical apertures naturally provide high effective gain and concentrated beams. However, these dishes are resource-inefficient due to mechanical steering and their limitation to supporting only a single satellite at a time. Large monolithic phased arrays offer an alternative by enabling multi-beam operation and fast electronic switching, but achieving dish-class gain (e.g., a 1.85 m dish) requires more than 50,000 antenna elements, making such systems impractical.

To achieve high-gain links in a practical and scalable manner, *ArrayLink* leverages commercial off-the-shelf phased array panels by coherently combining multiple smaller units, each contributing modest gain, into a coordinated network. In *ArrayLink*, each ground station comprises $N$ phased array panels. The total gain achieved by coherent combination can be expressed as:

$$\begin{aligned} G_{\text{total}} &= 10\log_{10}\left(N \cdot G_{\text{PA}} \cdot e^{-\delta}\right) \text{ dBi}, \\ &\approx 10\log_{10}(N) + G_{\text{PA}} \text{ (dB)}, \end{aligned} \tag{2}$$

where $G_{\text{PA}}$ denotes the gain of a single phased array panel, and $\delta$ accounts for synchronization losses due to phase misalignments across panels. Commercial satellite terminals from Starlink, Kuiper, OneWeb, and Telesat have already demonstrated the viability of planar phased arrays for dynamic, low-latency satellite access [33]–[35]. *ArrayLink* builds on this foundation by aggregating these smaller, commercially available arrays to achieve the higher gains required for robust backhaul links. This raises a key design question: *How many phased arrays are needed to reach dish-class performance while remaining practical and cost-effective?*

***Tradeoff between gain and practical feasibility:*** State-of-the-art phased arrays typically contain about 1,024 elements (e.g., $32 \times 32$), with individual microstrip antennas providing gains of approximately 6 dBi [36], [37], resulting in a total panel gain of about 36.1 dBi. As shown in Fig. 4a, achieving the gain of a 1.85 m dish requires at least 45 such panels, which limits scalability and introduces significant cost and system complexity. *ArrayLink* improves feasibility by reducing the number of required arrays at the cost of a small-gain tradeoff. The key insight is that the incremental gain from adding more arrays decreases exponentially, becoming negligible beyond a certain threshold. As illustrated in Fig. 4b, the marginal gain beyond 16 panels falls below 0.25 dB. Thus, instead of scaling to 45 panels, *ArrayLink* limits the aggregation to 16, reducing the array count by nearly two-thirds, allowing cost-efficient and scalable ground station deployments.

In summary, aggregating smaller phased arrays provides a practical strategy for scalable high-gain links, but naive scaling alone is inefficient. By trading a small amount of gain, *ArrayLink* ensures feasibility and cost effectiveness. The resulting reduction in per-link throughput compared to dishes is addressed in the next subsection, where *ArrayLink* leverages near-field MIMO techniques to unlock multiple concurrent spatial streams and scale overall throughput.

### *B. Near-Field MIMO: Unlocking Spatial Streams*

The key idea in this section is to investigate whether it is possible to maintain high throughput not by relying on a single high-SNR link, but by utilizing multiple spatial streams with lower individual SNRs. For example, instead of transmitting 6 bits per symbol using 64-QAM, one could transmit two parallel streams, each using lower-order modulation (e.g., 4–5 bits/symbol), and achieve comparable or higher aggregate throughput. This raises a central question: *how can we enable MIMO or support multiple spatial streams in satellite-to-ground feeder links where the channel is predominantly Line-of-Sight (LoS) and lacks rich scattering?*.

In conventional satellite links, the LoS-dominated channel leads to highly correlated entries in the MIMO channel matrix,

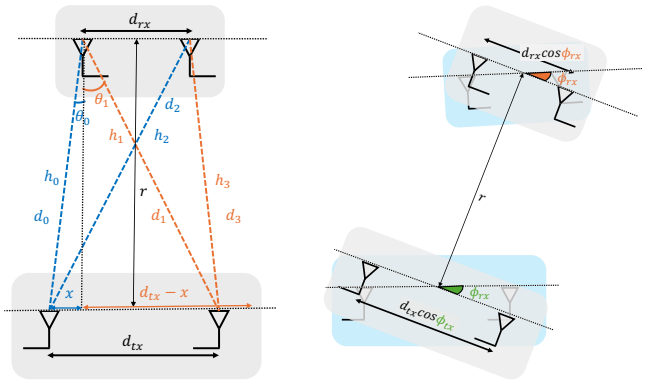


(a) 2×2 MIMO scenario with transmitter and receiver perpendicular to the LoS path.

(b) Virtual aperture sizes when transmitter and receiver deviate from perpendicular LoS.

Fig. 5: Line-of-sight (LoS) MIMO geometry with two transmit and two receive antennas.

rendering it ill-conditioned and rank-deficient. To assess feasibility, we consider a simplified 2×2 LoS MIMO system, shown in Fig. 5a, where both the transmitter and receiver employ two antennas. The channel matrix is $\mathrm{H} = \begin{pmatrix} h_0 & h_1 \\ h_2 & h_3 \end{pmatrix}$. where each channel coefficient is modeled as

$$h_i = \frac{\lambda}{\sqrt{4\pi d_i^2}} e^{-j\frac{2\pi d_i}{\lambda}}, \tag{3}$$

with $d_i$ denoting the path length between the corresponding transmit–receive antenna pair and $\lambda$ the carrier wavelength.

Beyond the Fresnel distance, $r_{\text{Fresnel}} = 0.62\sqrt{\frac{D^3}{\lambda}}$, the channel enters the radiative near-field regime, and beyond the Fraunhofer distance, $r_{\text{Far}} = 2D^2/\lambda$, it transitions to the far-field [8]. In both regimes, amplitude variations across antennas are negligible and phase differences dominate [38]. Accordingly, we normalize amplitudes and retain only phase terms: $h_i = e^{j\theta_i}$, $\theta_i = -\frac{2\pi d_i}{\lambda}$, $|h_i| = 1$. For this unit-modulus channel matrix, the singular values $\sigma_1, \sigma_2$ depend solely on the phase spread $\Delta$ (derivation in the appendix):

$$\sigma_{1,2} = \sqrt{2 \pm 2\left|\cos\frac{\Delta}{2}\right|}, \tag{4}$$

where $\Delta = (\theta_0 - \theta_2) - (\theta_1 - \theta_3)$. For the LoS geometry in Fig. 5a, the phase spread simplifies to

$$\begin{aligned} \Delta &= \frac{2\pi}{\lambda}\left[-(d_0 - d_2) + (d_1 - d_3)\right] \\ &= \frac{2\pi}{\lambda} d_{\text{rx}}\left[-\sin(-\theta_0) + \sin(\theta_1)\right] \\ &\approx \frac{2\pi}{\lambda} d_{\text{rx}}\left(\frac{x}{r} + \frac{d_{\text{tx}} - x}{r}\right) \\ &\approx 2\pi \cdot \frac{d_{\text{tx}} d_{\text{rx}}}{\lambda r}, \end{aligned} \tag{5}$$

where $d_{\text{tx}}$ and $d_{\text{rx}}$ are the transmit and receive antenna spacings, and $r$ is the distance between the transmitter and receiver centroids.

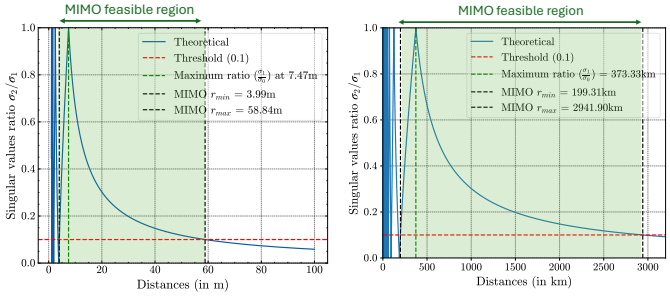


(a) $d_{\text{rx}} = 20cm$, $d_{\text{tx}} = 20cm$

(b) $d_{\text{rx}}$=$\sqrt{2}km$, $d_{\text{tx}}$=$\sqrt{2}m$

Fig. 6: Minimum and maximum distance boundaries for 2×2 LoS MIMO at (a) small and (b) satellite-scale apertures.

When the angles of departure and arrival deviate from 90°, the effective inter-element spacings shrink, as shown in Fig. 5b. The generalized phase spread becomes

$$\begin{aligned} \Delta &= 2\pi \frac{d_{\text{tx}}\cos(\phi_{\text{tx}})\; d_{\text{rx}}\cos(\phi_{\text{rx}})}{\lambda r} \\ &= 2\pi \frac{\tilde{d}_{\text{tx}}\tilde{d}_{\text{rx}}}{\lambda r}, \end{aligned} \tag{6}$$

where $\tilde{d}_{\text{tx}} = d_{\text{tx}}\cos(\phi_{\text{tx}})$ and $\tilde{d}_{\text{rx}} = d_{\text{rx}}\cos(\phi_{\text{rx}})$ denote the effective spacings. The remainder of this section focuses on the perpendicular LoS case, noting that other geometries follow directly by substituting these virtual spacings.

In summary, this formulation shows that the spacing between the transmit and receive antennas directly determines the phase spread, which in turn governs MIMO feasibility in LoS-dominated satellite links.

### *C. Boundaries for the MIMO Region: Minimum and Maximum Distance*

Having established that LoS MIMO can support multiple spatial streams, we now ask: *when can we enable MIMO reliably and what defines the boundaries of this MIMO region?* Unlike multipath-based MIMO, where feasibility depends on the propagation environment, near-field LoS MIMO is predictable. In this setting, the channel rank is determined solely by the transmit and receive antenna spacings ($d_{\text{tx}}, d_{\text{rx}}$) and their separation distance $r$.

Ideally, the singular values of $H$ should be nearly equal to maximize MIMO efficiency. From Eq. (4), this occurs when $\cos(\Delta/2) = 0$, i.e., $\Delta = \pi$. Since antenna spacings are fixed in practice, the singular-value ratio varies systematically with distance $r$, as illustrated in Fig. 6. Three regimes emerge:

- **Region 1** ($r < \frac{d_{\text{tx}} d_{\text{rx}}}{\lambda}$)**:** The singular-value ratio fluctuates rapidly between 0 and 1, making the channel highly sensitive to small geometric variations.
- **Region 2** ($\frac{d_{\text{tx}} d_{\text{rx}}}{\lambda} \le r \le \frac{2 d_{\text{tx}} d_{\text{rx}}}{\lambda}$)**:** The singular-value ratio increases monotonically from 0 to 1, yielding a stable and predictable MIMO region.
- **Region 3** ($r > \frac{2 d_{\text{tx}} d_{\text{rx}}}{\lambda}$)**:** The singular-value ratio decays gradually toward zero as distance increases.

A natural follow-up question is: What are the minimum and maximum distances that guarantee MIMO? To quantify MIMO

feasibility, we adopt a standard condition based on the singular-value ratio [39]. A 2×2 channel is considered well-conditioned for spatial multiplexing when

$$\frac{\sigma_{\min}}{\sigma_{\max}} > \tau \ (\tau \approx 0.1), \tag{7}$$

reflecting the requirement that spatial streams be sufficiently separable.

***Minimum distance.*** In Region 1, the singular-value ratio is unstable, making reliable MIMO operation difficult. Region 2 provides a stable operating regime. Using trigonometric identities, Eq. (4) reduces in this region to

$$\sigma_{max} = sin\frac{\Delta}{4}, \sigma_{min} = cos\frac{\Delta}{4}, \frac{\sigma_{min}}{\sigma_{max}} = cot\frac{\Delta}{4} \tag{8}$$

Combining Eqs. (5), (7), and (8) yields the minimum distance for stable MIMO:

$$r_{\min} = \frac{\pi}{2\arctan(1/\tau)} \frac{d_{\text{tx}} d_{\text{rx}}}{\lambda}. \tag{9}$$

***Maximum distance.*** In Region 3, as the distance increases, the condition number gradually reduces below the set threshold, making MIMO infeasible. As $\frac{\Delta}{4} < \frac{\pi}{4}$, the maximum and minimum singular values switch, i.e.

$$\sigma_{max} = cos\frac{\Delta}{4}, \sigma_{min} = sin\frac{\Delta}{4}, \frac{\sigma_{min}}{\sigma_{max}} = tan\frac{\Delta}{4} \tag{10}$$

Similar to the minimum distance, applying the feasibility criterion gives the maximum distance:

$$r_{\max} = \frac{\pi}{2\arctan(\tau)} \frac{d_{\text{tx}} d_{\text{rx}}}{\lambda} \approx \frac{\pi}{2\tau} \frac{d_{\text{tx}} d_{\text{rx}}}{\lambda}. \tag{11}$$

Therefore, two spatial streams are feasible for a $2 \times 2$ LoS MIMO system when $r_{\min} \leq r \leq r_{\max}$. Example operating points include:

- $d_{\text{tx}} = d_{\text{rx}} = 0.2\,\text{m}$, $\lambda = 0.01\,\text{m}$, $\tau = 0.1$, yielding $r \lesssim 62\,\text{m}$, consistent with our hardware measurements in Sec. IV-A.
- $d_{\text{tx}} = 2\,\text{km}$, $d_{\text{rx}} = 1\,\text{m}$ with the same $\lambda$ and $\tau$, yielding $r \approx 2500\,\text{km}$, representative of satellite feeder-link distances.

These bounds provide an analytical foundation for enabling near-field MIMO in LoS satellite links without relying on multipath scattering. By distributing phased-array panels, *ArrayLink* increases the effective ground-station aperture and creates a radiative near-field region that supports multiple spatial streams. However, large inter-panel spacings introduce grating lobes, which we discuss in the next subsection.

### *D. Phased array placement for reliable Beam focusing*

The previous sections show that distributing phased-array panels over kilometer-scale apertures enables near-field LoS MIMO. However, classical array theory predicts that uniform inter-element spacing beyond $\lambda/2$ introduces grating lobes, which appear to make coherent beamforming across kilometer-scale separations infeasible.

A key insight is that *ArrayLink* distributes *arrays rather than individual antennas*, decomposing beamforming into two separable components: (i) the intrinsic beamforming gain of each phased-array panel, and (ii) the array factor of a virtual array whose elements correspond to panel locations. As illustrated in Fig. 7, grating lobes (yellow) caused by large inter-panel spacing are strongly attenuated in off-target directions by the per-panel beam pattern (red). However, within the main lobe, residual grating lobes remain and manifest as a spatial sampling effect that cannot be eliminated by panel beamforming alone.

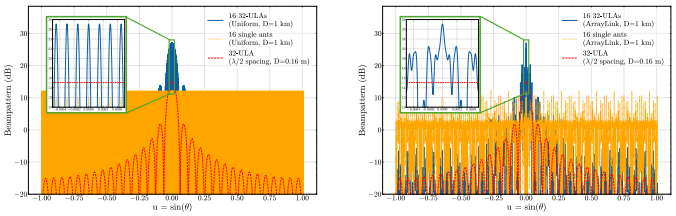


(a) Uniform placement within a 1 km aperture

(b) *ArrayLink* placement within a 1 km aperture

Fig. 7: Beam patterns with identical antenna counts comparing uniform and *ArrayLink* center-dense placement strategies.

For example, uniformly placing 16 panels across a 1 km aperture yields an inter-panel spacing of 62.5 m, corresponding to approximately $6000\lambda$ at 28 GHz. Such sparse uniform sampling produces an impulse-train-like array factor (Fig. 7a), causing the combined gain to oscillate rapidly with angle. Even a steering error as small as 0.002° can fall into a deep null, making the beam pattern highly sensitive and impractical for reliable operation.

*ArrayLink* alleviates this fundamental sampling effect through optimized non-uniform placement. Starting from uniform locations, *ArrayLink* applies a center-dense (power-law) transformation with randomized perturbations to reshape sidelobes from deterministic, periodic structures into low-amplitude, noise-like artifacts while preserving a dominant main lobe (Fig. 7b). In our design, the resulting beam pattern avoids abrupt transitions from high gain to deep nulls even under 0.01° pointing error, corresponding to approximately a 20× improvement in angular robustness. This enables stable, coherent beamforming over kilometer-scale apertures using a small number of distributed panels.

In general, achievable beamforming performance depends on panel placement, number of antenna elements, panel orientation, and the accuracy of satellite localization. A detailed exploration of these trade-offs is deferred to follow-up work.

## IV. Evaluations

To validate near-field MIMO feasibility in line-of-sight scenarios, we conducted both small-scale mmWave hardware experiments and large-scale simulations using a custom-built Python-based simulator.

### *A. Hardware setup*

**System Overview:** The testbed consists of one transmitter (TX) and one receiver (RX) node. Each node integrates two phase-coherent, vertically polarized $4 \times 8$ phased-array panels (64 elements each) connected to a single Ettus USRP B210

software-defined radio operating with a 3 GHz local oscillator (Fig. 8a). An external Analog Devices ADF5355 synthesizer provides a shared 6 GHz reference clock that is split and distributed to both panels, ensuring frequency coherence across arrays. The two panels on each node connect to the B210's dual RF ports, guaranteeing port-to-port timing alignment within the SDR. This configuration enables coherent operation at a carrier frequency of 27 GHz. All components are powered from a 12 V laboratory supply, and the B210 streams baseband I/Q samples to a host PC over USB 3.0, where GNU Radio performs real-time waveform generation on the TX side.

**Synchronization Strategy:** With the B210's internal VCXO bypassed, residual carrier-frequency offset (CFO) can exceed the tracking range of standard OFDM preambles. To coarsely align the radios, the transmitter emits a continuous 625 kHz tone while the receiver sweeps its center frequency until the FFT peak aligns with the tone, reducing CFO to within a few kilohertz. Any remaining offset is removed digitally during packet processing, enabling reliable demodulation of subsequent OFDM frames.

Notably, *ArrayLink* does not require tight phase synchronization between the transmitter and receiver. Instead, only synchronization among the receive chains is necessary. Our empirical measurements show that the relative phase offset between the two RF chains within the same SDR varies between 1° and 15°. Prior work has demonstrated wireless synchronization accuracy between phased arrays on the order of 2.26–20 ps [31], [32], which is well within the tolerance range of *ArrayLink*. As a result, *ArrayLink* remains robust to practical phase noise and residual synchronization errors.

**Receiver Processing:** A MATLAB supervisory script coordinates data acquisition at the receiver. It communicates with a background Python process interfacing with UHD to capture 50 bursts per run. For each burst, MATLAB performs packet detection, estimates and corrects fine CFO using the preamble, and extracts the $2 \times 2 \times 64$ channel frequency response. Channel measurements from all bursts are logged for subsequent analysis of channel conditioning and beamforming performance.

### B. Hardware experiments

We conducted hardware experiments in an open outdoor environment with a clear line-of-sight channel (Fig. 8b). Starting at a separation of 2.5 m, we collected 50 packets and computed the average singular-value ratio at that distance. The separation was then increased in 5 m increments up to 30 m, followed by 10 m increments up to 100 m.
At each distance, we evaluated four aperture configurations:

| Case | Transmit ($d_{tx}$ in cm) | Receive ($d_{rx}$ in cm) |
|---|---|---|
| 1 | 20 | 20 |
| 2 | 50 | 20 |
| 3 | 20 | 50 |
| 4 | 50 | 50 |

Fig. 10 plots the singular-value ratio $\sigma_2/\sigma_1$ as a function of transmitter–receiver distance, comparing hardware measurements, simulations, and theoretical predictions. For hardware experiments, the ratio is computed from measured $2 \times 2$ channel matrices extracted from 50 packets at each distance. Each marker denotes the mean singular-value ratio across packets, with the spread indicating the standard deviation. The small variance observed across all distances indicates a stable and predictable channel. Simulation results are obtained by evaluating Eq. (3) using the exact antenna coordinates in a 2×2 MIMO geometry, followed by singular value decomposition of the resulting channel matrix. Theoretical curves are generated using Eqs. (4) and (5), which express the singular values as a function of link distance, aperture size, and carrier wavelength.

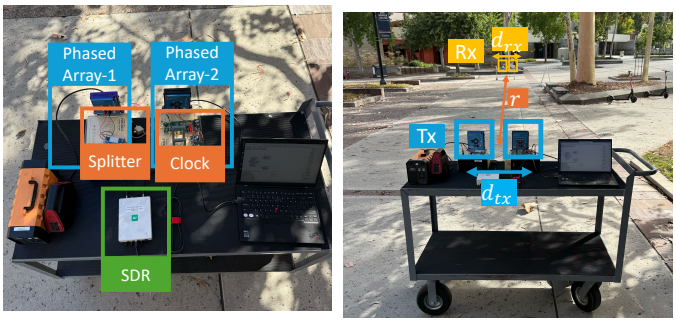


(a) Transmitter/Receiver setup: two phased arrays sharing same clock and SDR for data collection

(b) Experimental setup: Transmit and receive both with two phased in LoS.

Fig. 8: **Hardware setup:** Illustrating experimental setup for hardware experiment. Varied phased arrays separations ($d_{\text{tx}}$, ($d_{\text{rx}}$)) and distance ($r$) between transmitter and receiver.

Across all aperture configurations, hardware measurements closely track both simulation and theoretical results. The singular-value ratio remains above the feasibility threshold (highlighted by the green region) over a well-defined distance range, indicating a well-conditioned channel that supports spatial multiplexing. These results validate the feasibility of line-of-sight MIMO and demonstrate the ability to support multiple simultaneous spatial streams to a single transceiver in the mmWave band. More importantly, these small-scale measurements validate the analytical model and simulator, enabling reliable extrapolation to satellite-scale scenarios. More importantly, these small-scale measurements validate the analytical model and simulator, enabling reliable extrapolation to satellite-scale scenarios.

### C. Simulation Framework for Satellite–Ground Links

We develop a general-purpose Python simulator to analyze beamforming performance for arbitrary antenna configurations, including both monolithic arrays and distributed phased arrays. The simulator supports configurable antenna geometries, carrier frequency, satellite trajectories, and other related parameters. For *ArrayLink*, beamforming weights are computed using classical delay-and-sum phase compensation, following the optimal beamforming formulation in [40].
*Array Configurations:* We evaluate two representative deployment scenarios at 28 GHz ($\lambda \approx 10.7$ mm):

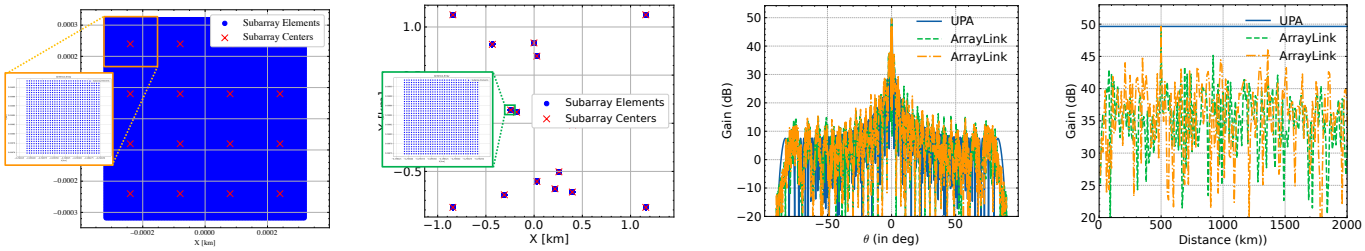


(a) 2D ULA with 128x128 antenna elements ($\lambda/2$ spacing).

(b) *ArrayLink*: 16 phased arrays (32x32 UPAs) positions.

(c) Beam pattern vs $\theta$ (with 16 - 32x32 phased arrays).

(d) Beam pattern vs distance (beam focusing in distance).

Fig. 9: **Simulation setup and results:** Antenna array placement for (a) 2D ULA with 128 x128 antenna elements and (b) *ArrayLink* with 16 32x32 distributed phased arrays in 2km x 2km grid.

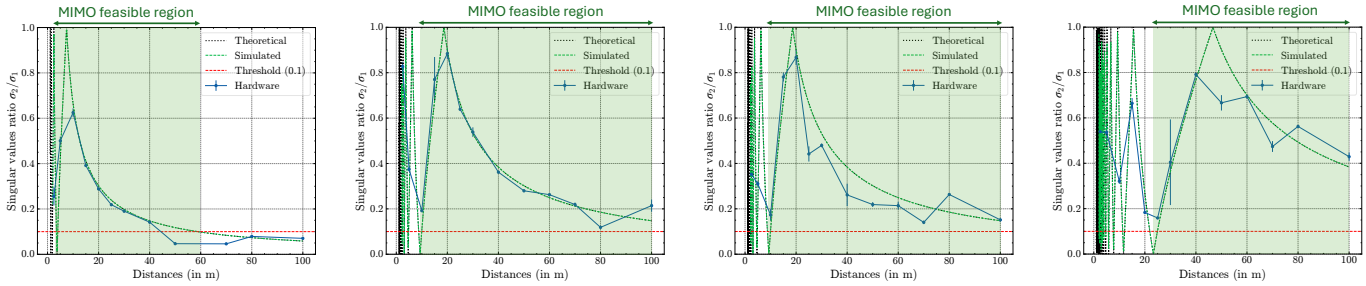


(a) $d_{\text{rx}} = 20cm, d_{\text{tx}} = 20cm$

(b) $d_{\text{rx}} = 20cm, d_{\text{tx}} = 50cm$

(c) $d_{\text{rx}} = 50cm, d_{\text{tx}} = 20cm$

(d) $d_{\text{rx}} = 50cm, d_{\text{tx}} = 50cm$

Fig. 10: **Hardware results:** Demonstrating that our hardware results (blue), closely match with both theory (eq-4,5) and simulate channel (eq-3) for different transmit ($d_{\text{tx}}$) and receive ($d_{\text{rx}}$) antenna separations (2x2 Scenario).

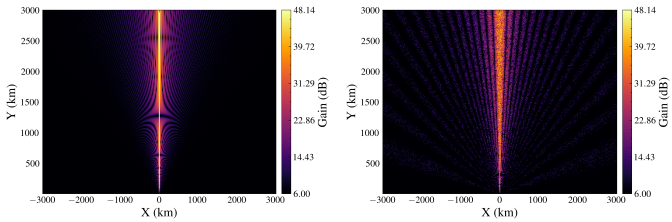


(a) Monolithic UPA

(b) *ArrayLink*

Fig. 11: Two-dimensional beam patterns over angle and range for (a) a monolithic UPA and (b) *ArrayLink* with distributed phased arrays over a 1.414 km × 1 km aperture.

- **Uniform Planar Array (UPA):** A monolithic $128 \times 128$ array with $\lambda/2$ element spacing (Fig. 9a).
- **Distributed Phased Arrays (*ArrayLink*):** Sixteen $32\times32$ phased-array panels distributed across a 1.414 km × 1 km aperture (Fig. 9b).

*1) Coherent Combining:* We compare *ArrayLink* 's coherent combining of sixteen $32 \times 32$ phased-array panels against a $128 \times 128$ UPA with the same total element count. Beamforming weights for both systems are computed using delay-and-sum phase alignment [40].

Fig. 9c shows array gain versus steering angle. Across all angles, *ArrayLink* achieves within 1–2 dB of the UPA, demonstrating near-parity in angular beamforming performance despite the distributed aperture. Fig. 9d plots gain versus range. While the UPA maintains a high and uniform gain across distance, *ArrayLink* concentrates energy both angularly and radially, suppressing off-target lobes outside the intended range.

Two-dimensional beam patterns in Fig. 11 further illustrate this behavior. The UPA exhibits a high-gain ridge at the steering angle that persists uniformly across range, whereas *ArrayLink* produces a localized gain peak that decays away from the focal range. This range localization not only preserves high on-axis gain for satellite links but also reduces off-axis interference. Overall, *ArrayLink* matches the high-gain beamforming of a monolithic UPA while additionally enabling distance-selective focusing, critical for interference mitigation in long-range satellite feeder links.

### *D. Line-of-Sight (LoS) MIMO Capability*

We further evaluate *ArrayLink* 's ability to support LoS MIMO on a satellite scale. As shown in Fig. 9b, sixteen $32 \times 32$ phased-array panels are distributed over a 1.414 km × 1 km ground aperture, while the satellite employs a four-element array arranged on a 1.414 m × 1 m grid. Using the channel model in Eq. (3), we compute the singular values of the resulting channel matrix and evaluate the achievable spatial degrees of freedom (DoF) over link distances up to 3,000 km.

Fig. 12a plots the ratios $\sigma_k/\sigma_1$ ($k = 2, 3, 4$) as a function of distance. A ratio exceeding the feasibility threshold indicates that the corresponding spatial stream is well conditioned. All three ratios remain above the threshold up to approximately 500 km, indicating support for four simultaneous streams. Beyond this range, the number of feasible streams decreases gradually: three streams remain viable up to roughly 1,000 km,

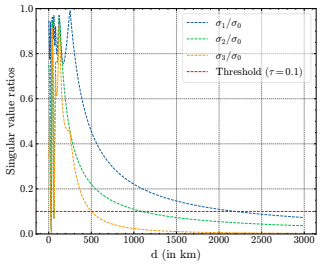


(a) Singular-value ratios indicating channel conditioning

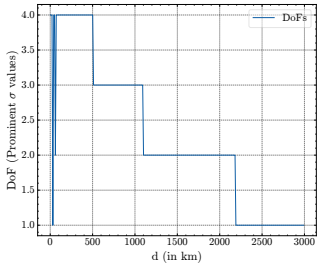


(b) Effective channel rank and number of feasible streams

Fig. 12: Simulation results demonstrating *ArrayLink* 's LoS MIMO capability with sixteen $32 \times 32$ phased-array panels distributed over a 1.414 km $\times$ 1 km ground aperture and a four-element satellite array arranged on a 1.414 m $\times$ 1 m grid.

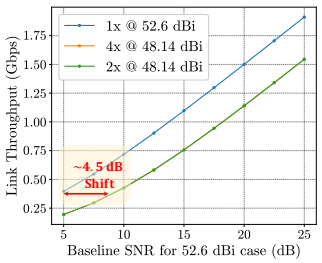


(a) Per-link throughput under varying SNR.

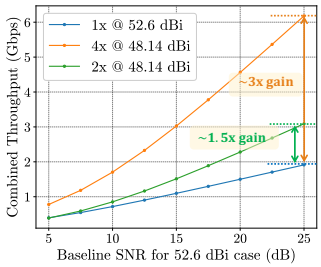


(b) Aggregate throughput across multiple spatial streams.

Fig. 13: Per-link and aggregate throughput with *ArrayLink*. Although per-link throughput decreases due to lower array gain, aggregate throughput increases by up to 50% with two streams and up to 200% with four streams.

and two streams persist beyond 2,000 km, as illustrated in Fig. 12b. These results confirm that *ArrayLink* not only achieves high-gain beamforming but also enables multiple concurrent spatial streams in line-of-sight satellite feeder links, significantly increasing aggregate throughput compared to traditional single-stream designs.

### *E. Throughput Improvement with Multiple Streams*

To evaluate the throughput gains from enabling multiple streams with *ArrayLink*, we compare against a 1.85 m parabolic dish baseline with 52.6 dBi gain. Due to feasibility tradeoffs, *ArrayLink* achieves a lower per-link gain of 48.14 dBi when aggregating 16 phased-array panels, corresponding to an effective SNR reduction of approximately 4.5 dB. Fig. 13a shows the per-link throughput as a function of SNR. As expected, the reduced array gain shifts the achievable per-link throughput downward relative to the dish baseline. However, Fig. 13b shows that enabling multiple streams significantly increases the aggregate capacity: by up to 50% (1.5×) with two streams and up to 200% (3×) with four streams. Importantly, this improvement reflects not only higher ground-station capacity but also increased end-to-end flow between satellites and ground stations.

In summary, *ArrayLink* scales aggregate throughput by up to 50% with two streams and 200% with four streams compared to a traditional parabolic dish, while requiring only 16 distributed phased arrays. This demonstrates that *ArrayLink* achieves the goal of high-throughput backhaul while maintaining practical feasibility, cost-effectiveness, and scalability.

## V. Conclusion

This paper presents *ArrayLink*, a scalable distributed phased-array ground station architecture that coherently combines commercially available panels to achieve dish-class beamforming gain without the cost, size, or rigidity of monolithic apertures. By distributing panels over a kilometer-scale aperture, *ArrayLink* operates in the radiative near field, enabling both high-gain beam-focused links and spatial multiplexing in line-of-sight satellite channels.

Evaluation through theoretical analysis, high-fidelity simulations, and outdoor experiments shows that near-field operation and array geometry, rather than dense uniform arrays, are the primary enablers of scalable capacity in satellite ground stations. Instead of relying on a single high-gain link, *ArrayLink* demonstrates that distributing modest-capability panels unlocks both beamforming gain and spatial degrees of freedom, fundamentally changing how ground-station throughput can be scaled under practical hardware constraints.

Future work will explore adaptive panel placement algorithms, validate the system with real-world LEO and GEO satellites, and extend the design to support multi-satellite operation for improved throughput, flexibility, and resilience.

## VI. Acknowledgements

We thank WCSNG team members at UC San Diego for their valuable feedback. This research was partially supported by the National Science Foundation grants 2232481 and 2211805.

## Appendix

Let

$$H = \begin{pmatrix} h_0 & h_1 \\ h_2 & h_3 \end{pmatrix}, \quad h_i = e^{-j\theta_i}, \quad |h_i| = 1.$$

The Frobenius norm is $\|H\|_F^2 = \sum_{i=0}^{3} |h_i|^2 = 4$. The determinant is

$$\det H = h_0 h_3 - h_1 h_2 = e^{-j(\theta_0+\theta_3)} - e^{-j(\theta_1+\theta_2)}.$$

Define

$$\alpha = \theta_0 + \theta_3, \quad \beta = \theta_1 + \theta_2, \quad \Delta = \alpha - \beta.$$

Then

$$|\det H| = \left|e^{-j\alpha} - e^{-j\beta}\right| = 2\left|\sin\frac{\Delta}{2}\right|.$$

The squared singular values satisfy the characteristic equation

$$\sigma^4 - \|H\|_F^2\,\sigma^2 + |\det H|^2 = 0,$$

$$\sigma_{1,2}^2 = \frac{\|H\|_F^2}{2} \pm \frac{1}{2}\sqrt{\|H\|_F^4 - 4|\det H|^2} = 2 \pm 2\left|\cos\frac{\Delta}{2}\right|.$$

Hence the singular values are

$$\sigma_{1,2} = \sqrt{2 \pm 2\left|\cos\tfrac{\Delta}{2}\right|}.$$

## References


[1] wiki, "*SpaceX.*" https://en.wikipedia.org/wiki/SpaceX, Aug 2025.

[2] ——, "*Planet Labs.*" https://en.wikipedia.org/wiki/Planet_Labs, Aug 2025.

[3] ——, "*Project Kuiper.*" https://en.wikipedia.org/wiki/Project_Kuiper, Aug 2025.

[4] ——, "*Eutelsat OneWeb.*" https://en.m.wikipedia.org/wiki/Eutelsat_OneWeb#OneWeb_satellite_constellation, Aug 2025.

[5] FCC, "*RADIO STATION AUTHORIZATION*," https://fcc.report/IBFS/SES-LIC-20200428-00458/3872480.pdf, Feb 2021.

[6] fcc, "*Application for Fixed Satellite Service by SpaceX Services, Inc.*" https://fcc.report/IBFS/SES-AMD-20230525-01127, Aug 2025.

[7] G. He, X. Gao, L. Sun, and R. Zhang, "A review of multibeam phased array antennas as leo satellite constellation ground station," *IEEE Access*, vol. 9, pp. 147 142–147 154, 2021.

[8] C. A. Balanis, *Antenna theory: analysis and design*. John wiley & sons, 2016.

[9] C. O. Systems, "*2.4AEBP-3m Elevation-Over-Azimuth Antenna Positioner*," https://www.orbitalsystems.com/wp-content/uploads/2020/06/2.4AEBP-3m-Data-Sheet-D.01.pdf, June 2025.

[10] V. Weerackody and L. Gonzalez, "Motion induced antenna pointing errors in satellite communications on-the-move systems," in *2006 40th Annual Conference on Information Sciences and Systems*. IEEE, 2006, pp. 961–966.

[11] M. Geng-Jun, X. Bin-Bin, W. Na, and W. Zhao-Jun, "Correction method of antenna pointing error caused by the main reflector deformation," *Chinese Astronomy and Astrophysics*, vol. 45, no. 2, pp. 236–251, 2021.

[12] Wikipedia, "*Phased array*," https://en.wikipedia.org/wiki/Phased_array, July 2025.

[13] J.-M. Kang, "Nmap-net: Deep learning-aided near-field multi-beamforming design and antenna position optimization for xl-mimo communications," *IEEE Internet of Things Journal*, 2025.

[14] K. Huang, J. Guan, Y. Wang, and X. Luo, "A symmetric beam training method for near-field xl-mimo systems," in *2025 6th International Conference on Electrical, Electronic Information and Communication Engineering (EEICE)*. IEEE, 2025, pp. 1491–1496.

[15] J. Li, Q. Chen, and F. Xi, "A blind super-resolution method for near-field channel estimation with angle-range recovery," in *ICASSP 2025-2025 IEEE International Conference on Acoustics, Speech and Signal Processing (ICASSP)*. IEEE, 2025, pp. 1–5.

[16] S. Liu, H. Wang, S. Li, J. Wang, H. Li, and F. Wang, "Gradient descent based polarization channel estimation in extremely largescale mimo systems," in *2025 IEEE 17th International Conference on Computer Research and Development (ICCRD)*. IEEE, 2025, pp. 155–160.

[17] H. Lei, J. Zhang, Z. Wang, B. Ai, and E. Bjornson, "Near-field user localization and channel estimation for xl-mimo systems: Fundamentals, recent advances, and outlooks," *IEEE Wireless Communications*, 2025.

[18] C. Zhou, C. You, S. Shi, J. Zhou, and C. Wu, "Super-resolution wideband beam training for near-field communications with ultra-low overhead," *IEEE Internet of Things Journal*, 2025.

[19] M. Liu, M. Li, R. Liu, and Q. Liu, "Dynamic hybrid beamforming designs for elaa near-field communications," *IEEE Journal on Selected Areas in Communications*, 2025.

[20] Q. Zhou, J. Zhao, K. Cai, and Y. Zhu, "Ris-assisted beamfocusing in near-field iot communication systems: A transformer-based approach," *IEEE Internet of Things Journal*, 2025.

[21] P. Sun and B. Wang, "Near-field beam-focusing for integrated sensing and communication systems," *IEEE Internet of Things Journal*, 2025.

[22] M. Cui, Z. Wu, Y. Lu, X. Wei, and L. Dai, "Near-field mimo communications for 6g: Fundamentals, challenges, potentials, and future directions," *IEEE Communications Magazine*, vol. 61, no. 1, pp. 40–46, 2022.

[23] M. Parvini, B. Banerjee, M. Q. Khan, T. Mewes, A. Nimr, and G. Fettweis, "A tutorial on wideband xl-mimo: Challenges, opportunities and future trends," *IEEE Open Journal of the Communications Society*, 2025.

[24] I. Sarris and A. R. Nix, "Maximum mimo capacity in line-of-sight," in *2005 5th International Conference on Information Communications & Signal Processing*. IEEE, 2005, pp. 1236–1240.

[25] K. Jiang, X. Wang, Y. Jin, A. Saleem, and G. Zheng, "Design and analysis of high-capacity mimo system in line-of-sight communication," *Sensors*, vol. 22, no. 10, p. 3669, 2022.

[26] R. Fernandez, Y. Ma, and R. Tafazolli, "Constellation with optimal leo spacing for satellite-to-mobile downlink communication," in *2024 IEEE-APS Topical Conference on Antennas and Propagation in Wireless Communications (APWC)*. IEEE, 2024, pp. 114–118.

[27] H. Pan, L. Qiu, B. Ouyang, S. Zheng, Y. Zhang, Y.-C. Chen, and G. Xue, "Pmsat: Optimizing passive metasurface for low earth orbit satellite communication," in *Proceedings of the 29th Annual International Conference on Mobile Computing and Networking*, 2023, pp. 1–15.

[28] M.-L. Chang, D.-B. Lin, H.-T. Rao, H.-Y. Lin, and H.-T. Chou, "Smart transfer planer with multiple antenna arrays to enhance low earth orbit satellite communication ground links." *Electronics (2079-9292)*, vol. 13, no. 17, 2024.

[29] I. Merino-Fernandez, S. L. Khemchandani, J. Del Pino, and J. Saiz-Perez, "Phased array antenna analysis workflow applied to gateways for leo satellite communications," *Sensors*, vol. 22, no. 23, p. 9406, 2022.

[30] C.-I. Adomnitei, C.-E. Lesanu, A. Done, E. Coca, and A. Lavric, "Phased antenna arrays, software defined radio and artificial intelligence: Advancing leo satellite communications," *Advances in Electrical and Computer Engineering*, vol. 24, no. 4, pp. 57–64, 2024.

[31] J. M. Merlo, S. R. Mghabghab, and J. A. Nanzer, "Wireless picosecond time synchronization for distributed antenna arrays," *IEEE Transactions on Microwave Theory and Techniques*, vol. 71, no. 4, pp. 1720–1731, 2022.

[32] K. Alemdar, D. Varshney, S. Mohanti, U. Muncuk, and K. Chowdhury, "Rfclock: Timing, phase and frequency synchronization for distributed wireless networks," in *Proceedings of the 27th Annual International Conference on Mobile Computing and Networking*, 2021, pp. 15–27.

[33] FCC, "*Spacex Purpose of Experiment*," https://apps.fcc.gov/els/GetAtt.html?id=259301, July 2025.

[34] Amazon, "*Here's your first look at Project Kuiper's low-cost customer terminals*," https://www.aboutamazon.com/news/innovation-at-amazon/heres-your-first-look-at-project-kuipers-low-cost-customer-terminals, March 2023.

[35] FCC, "*ONEWEB NON-GEOSTATIONARY SATELLITE SYSTEM (LEO)*," https://fcc.report/IBFS/SAT-MPL-20200526-00062/2379706.pdf, July 2025.

[36] E. Waves, "*SATCOM Ground Terminals*," https://www.extreme-waves.com/satcom, July 2025.

[37] Wikipedia, "*Microstrip antenna*," https://en.wikipedia.org/wiki/Microstrip_antenna, March 2025.

[38] Y. Liu, Z. Wang, J. Xu, C. Ouyang, X. Mu, and R. Schober, "Near-field communications: A tutorial review," *IEEE Open Journal of the Communications Society*, vol. 4, pp. 1999–2049, 2023.

[39] R. . Schwarz, "*Assessing a MIMO Channel - White Paper.*" https://scdn.rohde-schwarz.com/ur/pws/dl_downloads/dl_application/application_notes/8nt1/8NT1_0e_Assessing_MIMO_Ch.pdf, Aug 2025.

[40] H. L. Van Trees, *Optimum array processing: Part IV of detection, estimation, and modulation theory*. John Wiley & Sons, 2002.